

Easy-to-use formulations based on the homogenization theory for vascular stent design and mechanical characterization

*Original*

Easy-to-use formulations based on the homogenization theory for vascular stent design and mechanical characterization / Carbonaro, Dario; Ferro, Nicola; Mezzadri, Francesco; Gallo, Diego; Audenino, Alberto L.; Perotto, Simona; Morbiducci, Umberto; Chiastra, Claudio. - In: COMPUTER METHODS AND PROGRAMS IN BIOMEDICINE. - ISSN 0169-2607. - ELETTRONICO. - 257:(2024), pp. 1-10. [10.1016/j.cmpb.2024.108467]

*Availability:*

This version is available at: 11583/2999358 since: 2025-04-18T13:07:05Z

*Publisher:*

Elsevier

*Published*

DOI:10.1016/j.cmpb.2024.108467

*Terms of use:*

This article is made available under terms and conditions as specified in the corresponding bibliographic description in the repository

*Publisher copyright*

(Article begins on next page)



## Easy-to-use formulations based on the homogenization theory for vascular stent design and mechanical characterization

Dario Carbonaro<sup>a</sup>, Nicola Ferro<sup>b</sup>, Francesco Mezzadri<sup>c</sup>, Diego Gallo<sup>a</sup>, Alberto L. Audenino<sup>a</sup>, Simona Perotto<sup>b</sup>, Umberto Morbiducci<sup>a</sup>, Claudio Chiastra<sup>a,\*</sup>

<sup>a</sup> Department of Mechanical and Aerospace Engineering, Polito<sup>BIO</sup>Med Lab, Politecnico di Torino, Corso Duca degli Abruzzi, 24, Torino, Turin 10129, Italy

<sup>b</sup> MOX, Department of Mathematics, Politecnico di Milano, Milano, Italy

<sup>c</sup> Department of Engineering "Enzo Ferrari", University of Modena and Reggio Emilia, Modena, Italy

### ARTICLE INFO

#### Keywords:

Medical device design  
Auxetic stent  
Lattice structure  
Computational structural mechanics  
Finite element method  
Shape optimization  
Topology optimization

### ABSTRACT

**Background and objectives:** Vascular stents are scaffolding structures implanted in the vessels of patients with obstructive disease. Stents are typically designed as cylindrical lattice structures characterized by the periodic repetition of unit cells. Their design, including geometry and material characteristics, influences their mechanical performance and, consequently, the clinical outcomes. Computational optimization frameworks have proven to be effective in assisting the design phase of vascular stents, facilitating the achievement of enhanced mechanical performances. However, the reliance on time-consuming simulations and the challenge of automating the design process limit the number of design evaluations and reduce optimization efficiency. In this context, a rapid and automated method for the mechanical characterization of vascular stents is presented, taking the stent geometry, conceived as the periodic repetition of a unit cell, and material as input and providing the mechanical response of the stent as output.

**Methods:** Vascular stents were assumed to be thin-walled hollow cylinders sharing the same macroscopic geometrical characteristics as the cylindrical lattice structure but composed of an anisotropic homogenized material. Homogenization theory was applied to average the microscopic inhomogeneities at the stent unit cell level into a homogenized material at the macro-scale, enabling the calculation of the associated homogenized material tensor. Analytical formulations were derived to relate the stent mechanical behavior to the homogenized stiffness tensor, considering linear elastic theory for thin-walled hollow cylinders and three loading scenarios of relevance for vascular stents: radial crimping; axial traction; torsion. Validation was conducted by comparing the derived analytical formulations with results obtained from finite element analyses on typical stent designs.

**Results:** Homogenized stiffness tensors were computed for the unit cells of three stent designs, revealing insights into their mechanical performance, including whether they exhibit auxetic behavior. The derived analytical formulations were successfully validated with finite element analyses, yielding low relative differences in the computed values of foreshortening, radial, axial and torsional stiffnesses for all three stents.

**Conclusions:** The proposed method offers a rapid, fully automated procedure that facilitates the assessment of the mechanical behavior of vascular stents and is suitable for effective integration into computational optimization frameworks.

### 1. Introduction

Vascular stents are minimally invasive medical devices commonly used in the treatment of obstructive diseases [1]. Initially, stents undergo a crimping procedure (radial compression) for insertion into a

catheter. They are then deployed at the obstruction site in the vessel, with or without balloon expansion [2], to provide structural support to the vessel wall and prevent post-interventional vessel blockage [1]. Technically, vascular stents are designed as cylindrical lattice structures, typically characterized by the periodic repetition of a unit cell [1]. They

\* Corresponding author.

E-mail address: [claudio.chiastra@polito.it](mailto:claudio.chiastra@polito.it) (C. Chiastra).

<https://doi.org/10.1016/j.cmpb.2024.108467>

Received 21 August 2024; Received in revised form 3 October 2024; Accepted 16 October 2024

Available online 16 October 2024

0169-2607/© 2024 The Authors. Published by Elsevier B.V. This is an open access article under the CC BY-NC-ND license (<http://creativecommons.org/licenses/by-nc-nd/4.0/>).

come in various shapes, sizes, and materials depending on the target implantation site, whether it be the coronary, carotid, femoral arteries, or other locations [3–5].

The design of vascular stents, including cell geometry and material characteristics, directly influences the mechanical response of the devices and, consequently, the clinical outcomes [4–7]. Specifically, vascular stents require adequate radial stiffness to prevent vessel recoil while avoiding tissue damage [8]. Moreover, once implanted, they undergo mechanical loads such as radial loading, axial compression and tension, torsion, and bending, which vary according to the implantation site and tissue composition of the target vessel [9–11]. The mechanical response of a stent to this multifaceted loading condition determines the device-vessel interaction, which is a key design target for enhancing both the effectiveness and safety of the treatment, as well as for improving short- and long-term outcomes.

Computational modeling has proven effective in assisting the design and development of vascular stents, facilitating the achievement of designs with enhanced mechanical performances while reducing the need for prototyping and experimental testing [12]. Several computational design optimization frameworks have been developed for this purpose, employing either shape or topology optimization approaches to assess and balance competing design objectives, with the ultimate goal of enhancing clinical outcomes [6,13,22–29,14–21]. These optimization approaches involve iteratively evaluating the mechanical response of numerous stent designs. However, this iterative process is challenging to automate and typically relies on time-consuming structural mechanics analysis, thereby limiting the number of designs that can be evaluated and reducing the efficiency of the optimization frameworks.

In this context, this study introduces a method for the mechanical characterization of vascular stents through the analysis of periodic unit cell geometries. The proposed method exploits the homogenization theory combined with the linear elastic theory for thin-walled hollow cylinders to derive simple analytical formulations that relate specific stiffness tensor components to the mechanical behavior of the device. This method can be adopted to compare the mechanical responses expected from different stent unit cells designs and can be easily integrated into automated optimization frameworks to assist the preliminary design phase of new stents with improved mechanical performance.

## 2. Methods

The workflow of the proposed method for the evaluation of the mechanical performance of vascular stents with different unit cell

geometry is outlined in Fig. 1. In brief, the method takes the stent geometry, conceived as a periodic repetition of a unit cell, as input and provides a robust estimate of the foreshortening, radial, axial, and torsional stiffness values of the device as output. To achieve this, analytical formulations describing vascular stents mechanical behaviour are derived under three distinct loading conditions (i.e., radial compression, axial traction and torsion) using stiffness matrix components obtained combining the homogenization theory applied to the stent unit cell with the linear elastic theory for thin-walled hollow cylinders. Section 2.1 describes the general characteristics of the stent geometry and material. Section 2.2 details the evaluation of the homogenized stiffness tensor associated with the stent unit cell. Section 2.3 describes the assessment of the stent's mechanical properties based on the homogenized stiffness tensor and on the macroscopic geometric features of the device. Finally, Section 2.4 outlines the validation of the proposed framework through comparisons with finite element (FE) simulations, where the loading conditions of interest are applied to vascular stents featuring different unit cell geometries.

### 2.1. Vascular stent: geometry and mechanical response

Considering a cylindrical coordinate system, the typical geometry of a vascular stent can be conceptualized as comprising a 2D stent unit cell of constant thickness  $t$ , which is repeated periodically  $N_z$  times along the  $z$ -axis (i.e., the axial direction) and  $N_\theta$  times along the  $\theta$ -axis (i.e., the circumferential direction) to form the whole axisymmetric lattice structure (Fig. 2). Given the stent radius  $R_0$  and the aspect ratio  $\alpha = w/h$  of the unit cell (Fig. 2(a)), where  $w$  represents the width and  $h$  denotes the height of the unit cell, respectively, the length of the stent  $l_0$  can be determined according to the formula

$$l_0 = N_z w = N_z a h = 2\pi R_0 \alpha \frac{N_z}{N_\theta} \quad (1)$$

The mechanical response of vascular stents is determined by the associated design features, which include what we define (i) macroscopic quantities (i.e.,  $R_0$ ,  $l_0$ , and  $t$ ), (ii) microscopic quantities (i.e.,  $\alpha$ , and the unit cell topology), and (iii) the mechanical properties of the material employed for the device manufacturing. To account for all these design features within stent performance analysis in a computationally affordable way, the homogenization theory is applied to a 2D unit cell of the stent. To do that, vascular stents are assumed to be thin-walled hollow cylinders, macroscopically defined by  $R_0$ ,  $l_0$ , and  $t$ , and composed of an anisotropic homogenized material. This material is

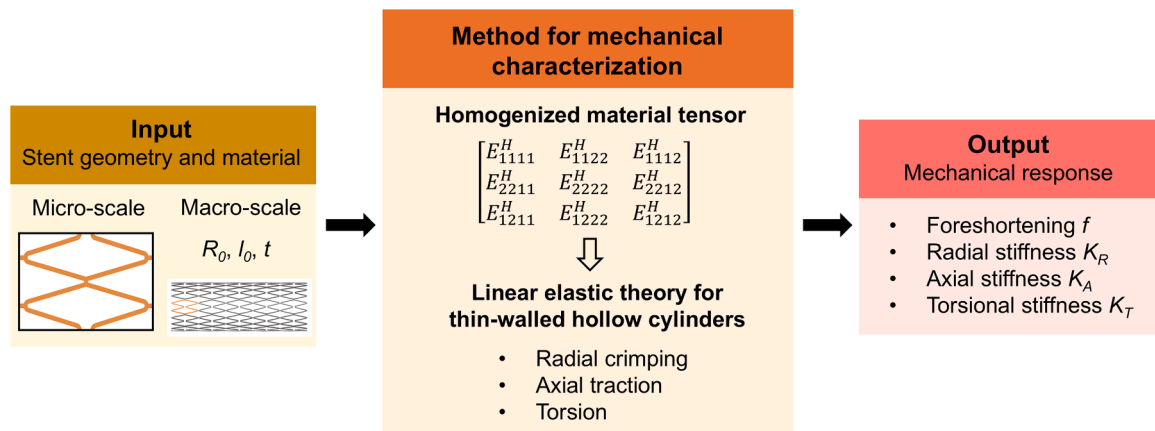
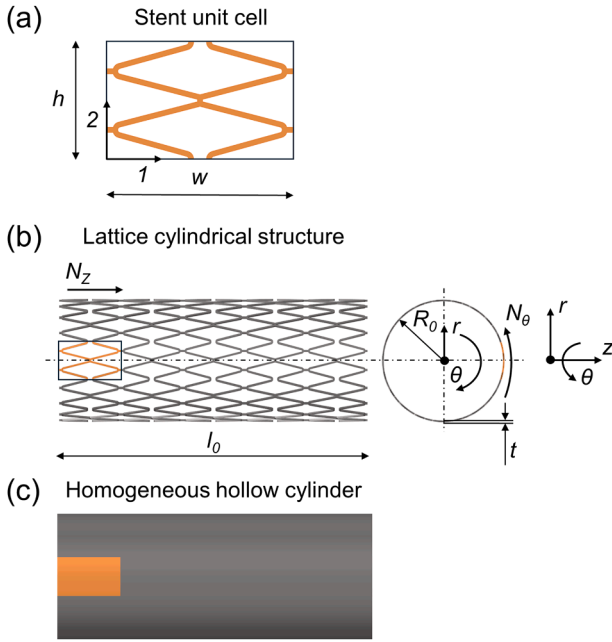


Fig. 1. Workflow of the method for the mechanical characterization of vascular stents. (i) Input: stent geometry conceived as the repetition of a unit cell (micro-scale geometric features) with specific values of radius  $R_0$ , length  $l_0$ , and thickness  $t$  (macro-scale geometric features), and material, as detailed in Section 2.1; (ii) Method for the mechanical characterization: evaluation of the homogenized material tensor corresponding to the investigated unit cell geometry, as detailed in Section 2.2, and application of linear elastic theory for thin-walled hollow cylinders under three distinct loading conditions, namely radial compression, axial traction and torsion, as detailed in Section 2.3; (iii) Output: evaluation of the mechanical response, including foreshortening  $f$ , radial stiffness  $K_R$ , axial stiffness  $K_A$ , and torsional stiffness  $K_T$ , as detailed in Section 2.3.



**Fig. 2.** (a) Stent unit cell, with indication of the local coordinate system;  $w$  and  $h$ : width and height of the unit cell, respectively. (b) Vascular stent, with indication of the global cylindrical coordinate system.  $N_z$  and  $N_\theta$ : number of periodic repetitions of the unit cell in  $z$  and  $\theta$  direction, respectively;  $t$ : thickness of the stent;  $l_0$ : length of the stent;  $R_0$ : radius of the stent, considering the radius of the inner and outer surfaces be equal to  $R_0 - t/2$  and  $R_0 + t/2$ , respectively. (c) Homogeneous thin-walled hollow cylinder with homogenized anisotropic material, with the same  $R_0$ ,  $l_0$  and  $t$ .

obtained by appropriately merging the microscopic quantities and unit cell topology of the 2D unit cell (Fig. 2(c)) with the mechanical properties of the manufacturing material.

## 2.2. Evaluation of the homogenized material tensor

Homogenization theory enables the rigorous simplification of a lattice structure characterized by repeated micro-scale unit cells (e.g., a stent), into a continuous model (e.g., a homogeneous continuous cylinder) effectively capturing the influence of microscale properties within the macroscopic characteristics (Fig. 2) [30]. To describe the homogenization technique in mathematical terms, it is assumed that the macroscopic medium under analysis,  $\Omega \subset \mathbb{R}^2$ , is the assembly of periodic repetitions of a microscopic unit cell,  $Y \subset \mathbb{R}^2$ , whose area  $|Y|$  is considerably lower than the area  $|\Omega|$  of the whole medium. Unit cells are not homogeneous, and this reflects in the microscopic variations in the physical behavior characterizing the macroscopic medium. The homogenization procedure removes such variations at the micro-scale, although inheriting the associated effect at the homogenized scale. With a view to the characterization of the mechanical properties of the stent, the reference physical model is the equilibrium elasticity equation at the macro-scale

$$-\nabla \cdot \sigma(\mathbf{u}) = 0 \text{ in } \Omega, \quad (2)$$

where  $\mathbf{u} \in \mathbb{R}^2$  is the displacement vector and  $\sigma$  is the stress tensor.

In a linear regime, the stress tensor is related to the strain tensor

$$\varepsilon(\mathbf{u}) = (\nabla \mathbf{u} + \nabla \mathbf{u}^T)/2$$

through the relation

$$\sigma(\mathbf{u}) = E\varepsilon(\mathbf{u}) = \begin{bmatrix} E_{1111} & E_{1122} & E_{1112} \\ E_{2211} & E_{2222} & E_{2212} \\ E_{1211} & E_{1222} & E_{1212} \end{bmatrix} \varepsilon(\mathbf{u}), \quad (3)$$

where the so-called stiffness tensor  $E = [E_{ijkl}]$ , with  $ij, kl \in \{11, 22, 12\}$ , is a symmetric fourth-order tensor depending on the considered material constituting the medium (i.e., Young's modulus and Poisson's ratio). Notice that Eq. (2) must be completed with appropriate boundary conditions on  $\partial\Omega$ , and that Eq. (3) is valid at both the macro-scale (in  $\Omega$ ) and the micro-scale (in  $Y$ ). Homogenization converts Eq. (3) to the homogenized counterpart

$$\sigma(\mathbf{u}) = E^H \varepsilon(\mathbf{u}), \quad (4)$$

where the homogenized stiffness tensors  $E^H$  links the mechanical response at the micro-scale  $Y$  to the macro-scale  $\Omega$ . In more detail, the stiffness tensor  $E^H$  can be obtained through an asymptotic expansion of the displacement field  $\mathbf{u}$  in Eq. (2) [30]. In practice, this leads to solve the following differential problem in the periodic unit cell  $Y$ : being  $U_P = [H_P^1(Y)]^2$  the vector space of periodic variations belonging to the Sobolev space  $H^1(Y)$ , and  $\mathbf{u}^{0,ij}$  denoting three independent test displacements, with  $\mathbf{u}^{0,11} = [x, 0]^T$ ,  $\mathbf{u}^{0,22} = [0, y]^T$ ,  $\mathbf{u}^{0,12} = [y, 0]^T$ , find the microscopic variations  $\mathbf{u}^{*,ij} \in U_P$ , with  $ij = \{11, 22, 12\}$  such that  $\forall v \in U_P$

$$\int_Y \sigma(\mathbf{u}^{*,ij}) : \varepsilon(v) dY = \int_Y \sigma(\mathbf{u}^{0,ij}) : \varepsilon(v) dY. \quad (5)$$

The solutions to Eq. (5) allow for the explicit expression of the homogenized stiffness tensor  $E^H = [E_{ijkl}^H]$ , where

$$E_{ijkl}^H = \frac{1}{|Y|} \int_Y [\sigma(\mathbf{u}^{0,ij}) - \sigma(\mathbf{u}^{*,ij})] : [\varepsilon(\mathbf{u}^{0,ij}) - \varepsilon(\mathbf{u}^{*,ij})] dY. \quad (6)$$

Eqs. (5) and (6) are commonly solved numerically. To this aim, a FE scheme based on adapted simplicial meshes and linear polynomials is adopted in this study to approximate variations  $\mathbf{u}^{*,ij}$  (namely to compute the stiffness tensor  $E^H$ ) in an accurate and efficient manner. We refer to [31] for the homogenization theory basics, and to recent literature for applications of adapted meshes to the computation of  $E^H$  [32–34].

## 2.3. Assessment of stent mechanical response

The mechanical response of vascular stents is here characterized considering three distinct loading scenarios (Fig. 3), namely (i) radial compression, (ii) axial tension, and (iii) torsion, enabling the evaluation of the device foreshortening  $f$ , radial stiffness  $K_R$ , axial stiffness  $K_A$ , and torsional stiffness  $K_T$ . The quantities  $K_R$  and  $f$  are evaluated by emulating radial compression (Fig. 3(a)) to replicate the radial crimping test, a standard procedure which mimics the loading conditions experienced by vascular stents when inserted into a catheter prior to deployment in the vessel [35,36]. The quantities  $K_A$  and  $K_T$  are evaluated by emulating axial traction and torsion tests, respectively (Fig. 3(b) and (c)).

The derivation of the analytical formulations expressing the mechanical response of the stents is performed by introducing some simplifying assumption. In detail, due to the small thickness  $t$  of the unit cells compared to  $R_0$  and  $l_0$ , the axisymmetric nature of vascular stents, and the boundary conditions characterizing the three loading scenarios, a state of plane stress is assumed with reference to the cylindrical coordinate system (Fig. 4). Moreover, since the radial crimping test aims to uniformly compress the vascular stent in the radial direction, the homogenized material tensor is assumed to be orthotropic, with negligible values for its components  $E_{1112}^H$  and  $E_{2212}^H$ , which couple normal strains  $\varepsilon_{\theta\theta}$  and  $\varepsilon_{zz}$  with the shear angle  $\gamma_{z\theta}$ : a not null value for the shear angle  $\gamma_{z\theta}$  implies the presence of out-of-plane strains and consequently, a non-uniform stent radial compression that may impact on the crimping

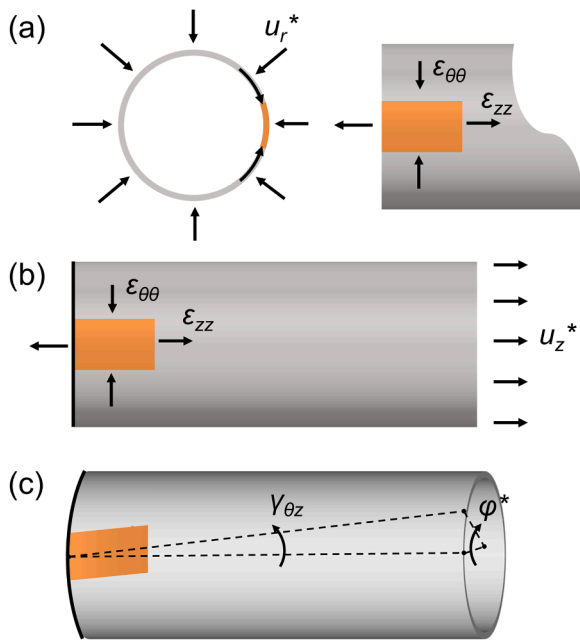


**Fig. 3.** Investigated loading scenarios with indication of the assigned boundary conditions. (a) Radial compression: a displacement  $u_r^*$  is assigned in the radial ( $r$ ) direction; accordingly,  $f$  and  $K_R$  are evaluated; (b) Axial traction: a displacement  $u_z^*$  is assigned in the axial ( $z$ ) direction at one extremity of the cylinder, while the other extremity (black line) is fixed in the  $z$  direction; accordingly,  $K_A$  is evaluated; (c) Torsion: a rotation  $\varphi^*$  is imposed on one extremity of the cylinder, while the other extremity (black line) is fixed in the circumferential ( $\theta$ ) direction; accordingly,  $K_T$  is evaluated.

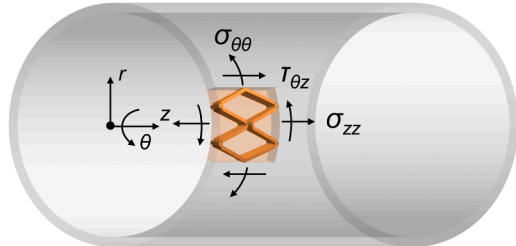


**Fig. 4.** Plane stress state in circumferential ( $\theta$ ) and axial ( $z$ ) directions for the investigated loading scenarios.

and deployment phases. Accordingly, in the cylindrical coordinate system of Fig. 4 the material constitutive relation of Eq. (4) in the plane 1–2 simplifies to

$$\begin{bmatrix} \sigma_{zz} \\ \sigma_{\theta\theta} \\ \tau_{z\theta} \end{bmatrix} = \begin{bmatrix} E_{1111}^H & E_{1122}^H & 0 \\ E_{2211}^H & E_{2222}^H & 0 \\ 0 & 0 & E_{1212}^H \end{bmatrix} \begin{bmatrix} \varepsilon_{zz} \\ \varepsilon_{\theta\theta} \\ \gamma_{z\theta} \end{bmatrix}. \quad (7)$$

Under an infinitesimal strain assumption, compatibility equations in the cylindrical coordinate system define the normal strains and the shear angle [37]

$$\begin{cases} \varepsilon_{\theta\theta} = \frac{1}{r} \frac{\partial u_\theta}{\partial \theta} + \frac{u_r}{r} \\ \varepsilon_{zz} = \frac{\partial u_z}{\partial z} \\ \gamma_{z\theta} = \frac{\partial u_z}{\partial \theta} + \frac{\partial u_\theta}{\partial z}, \end{cases} \quad (8)$$

with  $u_r$ ,  $u_\theta$ ,  $u_z$  the displacement components. Assuming that the axial symmetry of the stent is maintained in the examined loading scenarios (i.e., the cross-sections remain circular and normal to the  $z$ -axis), Eq. (8) simplifies to

$$\begin{cases} \varepsilon_{\theta\theta} = \frac{u_r}{r} \\ \varepsilon_{zz} = \frac{\partial u_z}{\partial z} \\ \gamma_{\theta z} = \frac{\partial u_\theta}{\partial z}. \end{cases} \quad (9)$$

The derivation of the analytical formulation for the estimate of the mechanical response of the stent is presented in the following subsections.

### 2.3.1. Radial stiffness and foreshortening

In the crimping test, the total force exerted by the device in the radial direction (i.e., the radial force) is quantified and used to determine the radial stiffness  $K_R$ , expressed as the ratio between the radial force and radial displacement. Radial stiffness is a fundamental mechanical requirement for vascular stents, as they must provide adequate scaffolding for the diseased vessel while minimizing the risk of damaging the arterial tissue [4,6]. Additionally, crimping a vascular stent might involve the elongation of device, which can be evaluated in terms of foreshortening

$$f = \frac{l - l_0}{l_0}, \quad (10)$$

where  $l$  is the stent length when radially compressed and  $l_0$  the device original length (Fig. 2(b)). The foreshortening  $f$  of the stent should be as small as possible to ensure precise placement during implantation [4,6]. Fig. 3(a) illustrates the boundary conditions prescribed for the radial compression. Specifically, a radial displacement  $u_r^*$  is prescribed on the entire cylindrical surface representing the stent. Consequently, the stress along the  $z$ -direction is identically null and the cylinder elongates at both ends in  $z$ -direction, reaching a length equal to  $l$ , with

$$\begin{cases} u_r = u_r^* \\ u_z = \frac{l - l_0}{l_0} \left( z - \frac{l_0}{2} \right), \end{cases} \quad (11)$$

for  $z \in [0, l_0]$ . Hence, from Eq. (9), it turns out that

$$\begin{cases} \varepsilon_{\theta\theta} = \frac{u_r^*}{R_0} \\ \varepsilon_{zz} = \frac{l - l_0}{l_0}, \end{cases} \quad (12)$$

and substituting the expressions for circumferential and axial strains (Eq. (12)) into Eq. (7) leads to the expression of the circumferential and axial stresses in terms of components of the homogenized stiffness matrix

$$\begin{cases} \sigma_{\theta\theta} = E_{1122}^H \varepsilon_{zz} + E_{2222}^H \varepsilon_{\theta\theta} \\ \sigma_{zz} = E_{1111}^H \varepsilon_{zz} + E_{1122}^H \varepsilon_{\theta\theta} = 0 \end{cases} \quad (13)$$

Finally, substituting Eq. (7) in Eq. (12) also allows the expression of foreshortening  $f$  in terms of the components of the homogenized stiffness matrix

$$f = \frac{l - l_0}{l_0} = -\frac{E_{1122}^H}{E_{1111}^H} \frac{u_r^*}{R_0}. \quad (14)$$

According to [38,39], the forces  $F_\theta$  (also known as hoop force) and  $F_r$  exerted by the vascular stent along the circumferential and the radial

direction, respectively, can be expressed

$$F_\theta = \sigma_{\theta\theta} l_0 t, \quad (15)$$

$$F_r = 2\pi F_\theta = 2\pi\sigma_{\theta\theta} l_0 t. \quad (16)$$

Therefore, by definition,  $K_R$  can be also expressed in terms of components of the homogenized stiffness matrix

$$K_R = \frac{F_r}{u_r^*} = \frac{2\pi l_0 t}{R_0} \left( E_{2222}^H - \frac{(E_{1122}^H)^2}{E_{1111}^H} \right) = K_R^M K_R^m, \quad (17)$$

where

$$\begin{cases} K_R^M = \frac{2\pi l_0 t}{R_0} \\ K_R^m = E_{2222}^H - \frac{(E_{1122}^H)^2}{E_{1111}^H}, \end{cases} \quad (18)$$

represent the radial stiffness related to the macroscopic ( $K_R^M$ ) and microscopic ( $K_R^m$ ) scales of the stent.

### 2.3.2. Axial stiffness

The axial stiffness  $K_A$  can be evaluated as the ratio between the force exerted by the device in the axial direction (i.e., the axial force) and the imposed axial displacement. Fig. 3(b) illustrates the boundary conditions applied when axial displacement is prescribed to evaluate  $K_A$ . Specifically, an axial displacement  $u_z^*$  is imposed on one extremity of the cylinder, while the other extremity is fixed in the  $z$ -direction, namely

$$u_z = \frac{u_z^*}{l_0} z, \quad (19)$$

with  $z \in [0, l_0]$ . From Eq. (9), it follows that

$$\varepsilon_{zz} = \frac{u_z^*}{l_0}. \quad (20)$$

Substituting Eq. (20) into Eq. (7) yields the expression of the axial and circumferential stresses in terms of components of the homogenized stiffness matrix

$$\begin{cases} \sigma_{zz} = E_{1111}^H \varepsilon_{zz} + E_{1122}^H \varepsilon_{\theta\theta} \\ \sigma_{\theta\theta} = E_{1122}^H \varepsilon_{zz} + E_{2222}^H \varepsilon_{\theta\theta} = 0, \end{cases}$$

where the stress  $\sigma_{\theta\theta}$  is identically null because the cylinder is kept traction-free in the radial direction. Following [38], it turns out that the total axial force  $F_z$  can be expressed

$$F_z = \sigma_{zz} \pi \left[ \left( R_0 + \frac{t}{2} \right)^2 - \left( R_0 - \frac{t}{2} \right)^2 \right] = \sigma_{zz} 2\pi R_0 t. \quad (21)$$

Therefore, by definition,  $K_A$  can be expressed in terms of the components of the homogenized stiffness matrix

$$K_A = \frac{F_z}{u_z^*} = \frac{2\pi R_0 t}{l_0} \left( E_{1111}^H - \frac{(E_{1122}^H)^2}{E_{2222}^H} \right) = K_A^M K_A^m, \quad (22)$$

where

$$\begin{cases} K_A^M = \frac{2\pi R_0 t}{l_0} \\ K_A^m = E_{1111}^H - \frac{(E_{1122}^H)^2}{E_{2222}^H}, \end{cases} \quad (23)$$

represent the axial stiffness related to the macroscopic ( $K_A^M$ ) and

microscopic ( $K_A^m$ ) scales of the stent.

### 2.3.3. Torsional stiffness

The torsional stiffness  $K_T$  can be evaluated as the ratio between the total torque moment exerted by the device around the axial direction and the imposed rotation around the same direction. Fig. 3(c) illustrates the boundary conditions applied when a rotation around the axial direction is prescribed to evaluate  $K_T$ . Specifically, a rotation  $\varphi^*$  is imposed on one extremity of the cylinder, while the other extremity is fixed along the  $\theta$ -direction, yielding to a circumferential displacement

$$u_\theta^* = R_0 \varphi^* \frac{z}{l_0}, \quad (24)$$

with  $z \in [0, l_0]$ . From Eqs. (7) to (9), it follows that

$$\gamma_{\theta z}^* = \frac{R_0}{l_0} \varphi^*, \quad (25)$$

$$\tau_{\theta z} = E_{1212}^H \gamma_{\theta z}^*. \quad (26)$$

As in [38], the torque moment  $M_z$  can be expressed in the following terms

$$M_z = \frac{\pi}{2R_0} \left[ \left( R_0 + \frac{t}{2} \right)^4 - \left( R_0 - \frac{t}{2} \right)^4 \right] \tau_{\theta z}. \quad (27)$$

Therefore, using Eq. (27), the torsional stiffness  $K_T$  can be expressed in terms of the components of the homogenized stiffness matrix

$$K_T = \frac{M_z}{\varphi^*} = \frac{\pi(4R_0^3 t + R_0 t^3)}{2l_0} E_{1212}^H = K_T^M K_T^m \quad (28)$$

where

$$\begin{cases} K_T^M = \frac{\pi(4R_0^3 t + R_0 t^3)}{2l_0} \\ K_T^m = E_{1212}^H, \end{cases} \quad (29)$$

represent the torsional stiffness related to the macroscopic ( $K_T^M$ ) and microscopic ( $K_T^m$ ) scales of the stent.

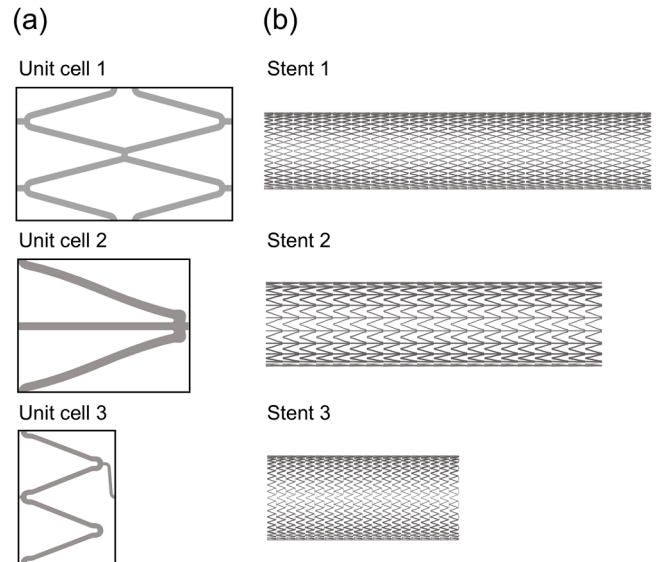


Fig. 5. (a) Stents unit cells; (b) FE models of stents corresponding to the unit cells in (a), when considering  $N_z = N_\theta = 20$ ,  $t = 0.1$  mm,  $R_0 = 3.5$  mm.

## 2.4. Numerical experiments

The analytical formulations derived to express  $f$ ,  $K_R$ ,  $K_A$  and  $K_T$  in terms of the components of the homogenized stiffness matrix are tested against FE simulations where the three loading scenarios are applied to vascular stent designs modelled as cylindrical lattice structures. For this purpose, three stent unit cell types resembling commercially available self-expandable femoral stent designs are considered (Fig. 5(a)). Subsequently, the homogenized stiffness tensor is determined for each one of the three analyzed unit cell designs, and  $f$ ,  $K_R$ ,  $K_A$  and  $K_T$  are evaluated using the derived analytical formulations (Eqs. (14), (17), (22) and (28)). In parallel, FE models of the three vascular stent designs are generated by periodically repeating the unit cells in the axial and circumferential directions (Fig. 5(b)), and  $f$ ,  $K_R$ ,  $K_A$  and  $K_T$  are computed based on the FE analysis. Finally, the results from analytical formulations and from FE simulations are compared. The analysis was performed assuming that vascular stents are fabricated from Nickel-Titanium (Young's modulus equal to 60 GPa and Poisson's ratio equal to 0.33 [15]) with the following macroscopic geometrical characteristics:  $R_0 = 3.5$  mm,  $t = 0.1$  mm,  $N_\theta = N_z = 20$ . Furthermore, a sensitivity analysis of the derived analytical formulations with respect to the design parameters  $N_\theta$  and  $N_z$  is performed. To address this task, FE models are developed for unit cell type 1.

### 2.4.1. Stent unit cell geometries

Fig. 5 displays the three stent designs with different unit cell types selected for the analysis, each resembling commercially available self-expandable femoral stents. Unit cell 1 is inspired by the EverFlex stent (Medtronic, Dublin, Ireland), unit cell 2 by the Zilver PTX stent (Cook Medical, Bloomington, IN, USA), and unit cell 3 by the S.M.A.R.T. Vascular System (S.M.A.R.T., Santa Clara, CA, USA). The unit cells 1, 2 and 3 are assumed to have a unitary height  $h$  (Fig. 2(a)) and an aspect ratio  $\alpha$  equal to 1.62, 1.28, and 0.73, respectively. In addition, the unit cells have a volume fraction, defined as the ratio of the area covered by the stent unit cell to the total area of the unit cell [15], of 19%, 19% and 15%, respectively. For each unit cell, the homogenized stiffness tensor is reconstructed as detailed in Section 2.1.

### 2.4.2. FE analysis

FE models for stent mechanical characterization are created starting from the unit cell geometries by using Hypermesh (Altair Engineering, Troy, MI, USA) and Abaqus/Standard (Dassault Systemes Simulia Corp., Johnston, RI, USA). The unit cells (Fig. 5(a)) are meshed with four-nodes shell elements S4R, considering eight elements along the strut width. Grid element size is the result of a mesh grid independence study, detailed in the Supplementary material. Linear structural mechanics FE analysis is carried out adopting the implicit solver Abaqus/Standard, running on 6 computing cores of a workstation equipped with Intel® Core™ i7-8700 and 32 GB RAM. Boundary conditions for the three distinct loading scenarios (i.e., radial, axial traction, and torsion loading) are applied as described in Fig. 3. Reaction forces and moments are computed to determine  $K_R$ ,  $K_A$  and  $K_T$ . Specifically, for the radial compression scenario, a radial displacement of  $u_r^* = 0.25$  mm is prescribed to all the nodes of the stent and  $F_r$  is computed as the sum of the nodal reaction forces in the  $r$ -direction (see Eq. (11)). For the axial traction scenario, a displacement  $u_z^* = 0.1$  mm is prescribed to the nodes at one extremity of the stent, while the nodes at the other extremity are fixed in the  $z$ -direction, and  $F_z$  is computed as the sum of the nodal reaction forces in  $z$ -direction (see Eq. (19)). For the torsion scenario, two kinematic coupling elements are adopted, each connecting the nodes at one extremity of the stent, with their master nodes aligned along the  $z$ -axis. A rotation of  $\varphi^* = 10^\circ$  is prescribed to one master node, while the other master node is constrained in rotation about the  $z$ -axis, and  $M_z$  is computed as the reaction moment at the constrained master node (see Eq. (24)). Notice that the specific values adopted for  $u_r^*$ ,  $u_z^*$ , and  $\varphi^*$  are compliant with the assumption of infinitesimal strains.

Additional details regarding the FE analysis are provided in the Supplementary material.

## 3. Results

### 3.1. Homogenized stiffness tensor

As the first result, we present the homogenized stiffness tensors for the three stent designs with unit cell types of Fig. 5(a), obtained using the method proposed here:

$$E^H = \begin{bmatrix} 428.425 & 38.608 & 0.072 \\ 38.608 & 8.723 & 0.007 \\ 0.072 & 0.007 & 12.472 \end{bmatrix} \text{ (MPa), for unit cell 1;}$$

$$E^H = \begin{bmatrix} 3615.720 & -0.054 & 0.102 \\ -0.054 & 3.317 & -0.006 \\ 0.102 & -0.006 & 4.734 \end{bmatrix} \text{ (MPa), for unit cell 2;}$$

$$E^H = \begin{bmatrix} 15.590 & 1.845 & 0.349 \\ 1.845 & 5.367 & -1.090 \\ 0.349 & -1.090 & 3.609 \end{bmatrix} \text{ (MPa), for unit cell 3.}$$

Based on the obtained homogenized stiffness tensors, Table 1 summarizes the values of the mechanical response of the stents corresponding to the investigated unit cells, evaluated adopting the analytical formulations derived in Section 2.3. From the analysis it emerges that while the values of the radial and the torsional stiffness at the micro-scale are of the same order of magnitude for the three cell unit types, the axial stiffness varies considerably, from 15.0 MPa (unit cell type 3) to 3615.7 MPa (unit cell type 2). Additionally, the stent made by unit cells type 2 demonstrates auxetic properties, with a negative, near zero value of  $f$ , markedly lower compared to the other stents.

### 3.2. Derived analytical formulations vs. FE analysis

The paired comparison between the values of  $f$ ,  $K_R$ ,  $K_A$  and  $K_T$ , as evaluated using the derived analytical formulations and the FE analysis, is summarized in Fig. 6 for the three different unit cell types-based devices. A satisfactory agreement emerges between the two sets of values. Specifically, the relative differences between the analytical formulation and the FE analysis are up to 6% for  $K_R$  ([3% - 6%]) and up to 4% for  $K_A$  ([2% - 4%]). As for  $K_T$ , differences up to 18% emerge ([2% - 18%]). The largest deviation is observed for the foreshortening  $f$ , with differences less than 6% for stents with unit cell types 1 and 3, but up to 49% for the device relative to unit cell type 2, which is attributed to the very small value obtained for  $f$ , which is close to zero ( $f = -10^{-4}$  %).

The results of the sensitivity analysis for  $f$ ,  $K_R$ ,  $K_A$ , and  $K_T$ , evaluated using the derived analytical formulations, with respect to the geometric parameters  $N_z$  and  $N_\theta$  are presented in Fig. 7 for the stent design based on the unit cell type 1, accompanied by the paired values from the FE analysis. Overall, a close agreement emerges across the considered ranges of variations for  $N_z$  and  $N_\theta$ , between values obtained from the analytical formulations and those derived from the 3D FE models. Specifically, relative differences are approximately 6% and 3% for  $f$  and  $K_A$ , respectively (Fig. 7(a) and (c)). Regarding the calculation of  $K_R$ , the relative difference is reduced from approximately 6% to 2% when increasing  $N_\theta$  from 10 to 40, for all the  $N_z$  values (Fig. 7(b)). Finally, regarding the calculation of  $K_T$ , the relative difference decreases from approximately 19% to 5%, from 17% to 5%, and from 16% to 4%, by varying  $N_z$  from 10 to 40, for  $N_\theta = 10$ ,  $N_\theta = 20$ , and  $N_\theta = 40$ , respectively (Fig. 7(d)).

## 4. Discussion

Computational models have proven to be efficient tools for assisting the design phase of vascular stents, enabling the optimization of the

**Table 1**

Mechanical response of the stents associated with the three stent designs with different unit cell types in Fig. 5(a), evaluated using the derived analytical formulations considering  $N_\theta = N_z = 20$ ,  $R_0 = 3.5$  mm, and  $t = 0.1$  mm.

	$\alpha$	$l_0$ (mm)	$f$ (%)	Radial crimping			Axial traction			Torsion		
				$K_R^m$ (MPa)	$K_R^M$ (mm)	$K_R$ (N/mm)	$K_A^m$ (MPa)	$K_A^M$ (mm)	$K_A$ (N/mm)	$K_T^m$ (MPa)	$K_T^M$ (mm <sup>3</sup> )	$K_T$ (N mm)
Stent 1	1.62	35.6	6.1	5.2	6.39	33.5	257.5	0.06	15.7	12.5	0.77	9.4
Stent 2	1.28	28.1	$-10^{-4}$	3.3	5.04	16.8	3615.7	0.08	278.4	4.7	0.98	4.5
Stent 3	0.73	16.1	0.85	5.2	2.89	14.8	15.0	0.14	2.0	3.6	1.71	6.1

$\alpha$ : aspect ratio of the unit cell;  $K_R^m$ : radial stiffness of the stent at the micro-scale;  $K_R^M$ : radial stiffness of the stent at the macro-scale;  $K_R$ : radial stiffness of the stent;  $K_A^m$ : axial stiffness of the stent at the micro-scale;  $K_A^M$ : axial stiffness of the stent at the macro-scale;  $K_A$ : axial stiffness of the stent;  $K_T^m$ : torsional stiffness of the stent at the micro-scale;  $K_T^M$ : torsional stiffness of the stent at the macro-scale;  $K_T$ : torsional stiffness of the stent.

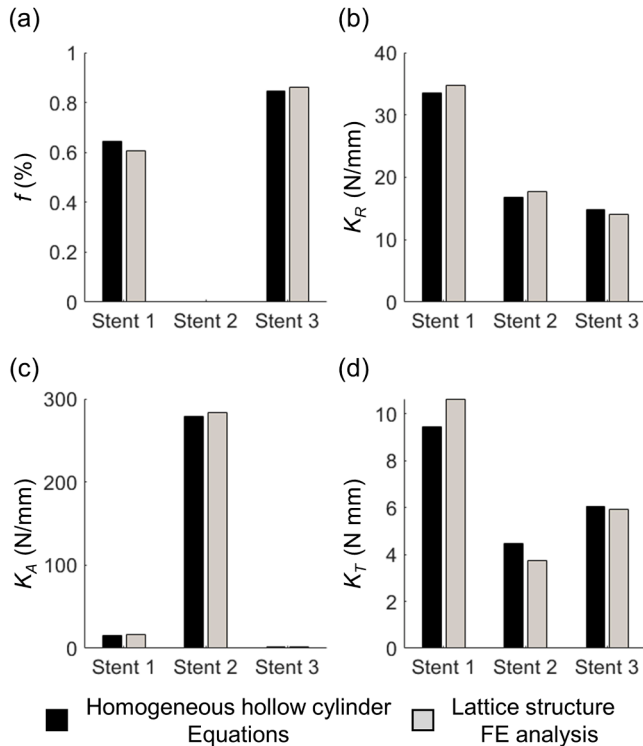


**Fig. 6.** Values of (a)  $f$ , (b)  $K_R$ , (c)  $K_A$  and (d)  $K_T$  computed using the derived analytical formulations as well as by FE analysis for the investigated stents, made of three different unit cell types.  $f$ : foreshortening;  $K_R$ : radial stiffness;  $K_A$ : axial stiffness;  $K_T$ : torsional stiffness;  $N_z$  and  $N_\theta$ : number of repetitions of the unit cell in  $z$  and  $\theta$  directions, respectively. For the sake of comparison, vascular stents were considered with the following macroscopic geometrical characteristics:  $R_0 = 3.5$  mm,  $t = 0.1$  mm,  $N_\theta = N_z = 20$ .

mechanical response, with the ultimate goal of enhancing treatment safety and efficiency [6,13,22–29,14–21]. In this context, the present study contributes to the advancement of vascular stent design and performance analysis by exploring the relationship between stent unit cell attributes and stent mechanical response, thereby facilitating the optimization of the mechanical performance. The analytical formulations derived here effectively describe the mechanical behavior of the stent through a combination of stiffness matrix components obtained using a through-scales homogenization strategy. The proposed method promises to become an easy-to-use, automated tool supporting stents design and optimization, reducing the need for expensive 3D structural mechanics simulations. This is achieved by performing homogenization analysis on the 2D unit cell, which has already been proven to be fully automatable. In this regard, starting from an imported unit cell geometry, the overall procedure takes < 5 min to evaluate the mechanical behavior of the stent on a standard laptop (Intel<sup>(R)</sup> Core<sup>TM</sup> i7–1165G7

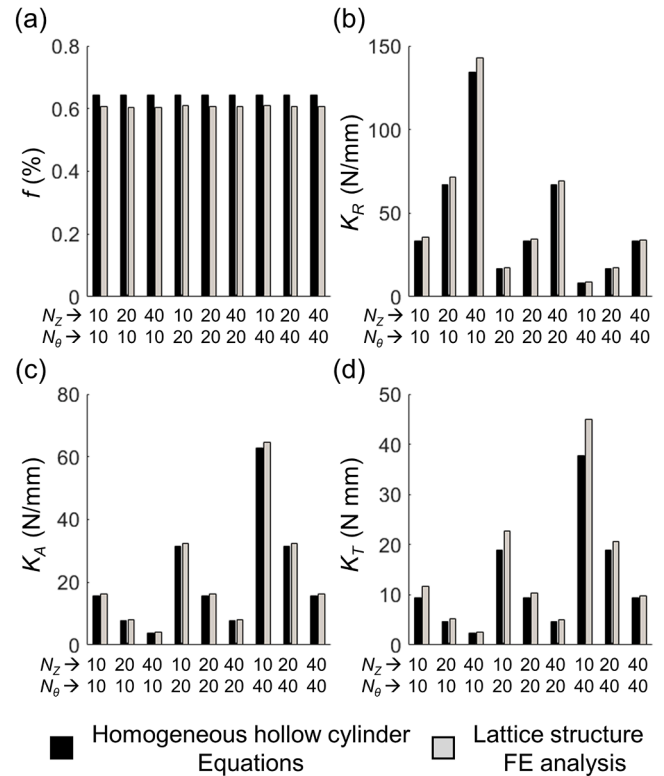


**Fig. 7.** Values of (a)  $f$ , (b)  $K_R$ , (c)  $K_A$  and (d)  $K_T$  evaluated using the derived analytical formulations along with the corresponding values provided by the FE analysis for the stent design corresponding to unit cell type 1, when considering different values of  $N_z$  and  $N_\theta$ .  $f$ : foreshortening;  $K_R$ : radial stiffness;  $K_A$ : axial stiffness;  $K_T$ : torsional stiffness.  $N_z$  and  $N_\theta$ : number of repetitions of the unit cell in  $z$  and  $\theta$  direction, respectively. For the sake of comparison, vascular stents were assumed to have the following macroscopic geometrical characteristics:  $R_0 = 3.5$  mm and  $t = 0.1$  mm.

and 8 GB RAM). Thus, the procedure is well-suited for integration into computational optimization frameworks. In particular, shape optimization frameworks for vascular stents typically consider an initial geometry with a set of parameterized geometric features, which are explored within the design space to enhance the device’s mechanical performance [6]: the proposed procedure can be adopted to automatically evaluate a set of unit cells, or it can be incorporated in the optimization iterative routine to link the geometrical attributes of the unit cell to optimization objectives (Fig. 8). Additionally, topology optimization frameworks for vascular stents generally aim to iteratively determine the optimal material distribution to meet specific design requirements without relying on an initial predefined stent geometry, resulting in a more general approach with the potential to generate innovative geometries [6]. Specifically, a recent study [15] has

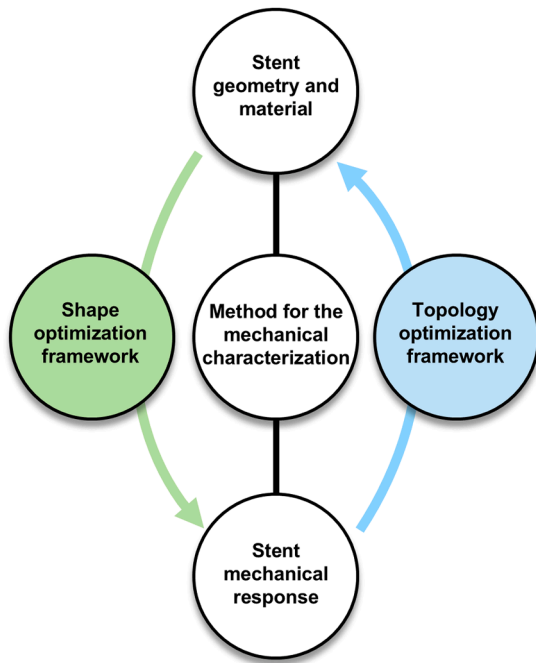


Fig. 8. Implementation of the proposed approach within stent optimization frameworks.

exploited topology optimization for designing innovative stent unit cells that match specific values of homogenized stiffness tensor components. The capability of this framework can be extended to link  $f$ ,  $K_R$ ,  $K_A$ , and  $K_T$  of the stent with the homogenized material tensor, enabling the generation of optimal unit cell geometries that meet specific mechanical requirements (Fig. 8).

The derived analytical formulations for  $f$ ,  $K_R$ ,  $K_A$  and  $K_T$  have been successfully tested against FE simulations considering three different stent unit cell designs resembling commercial devices. In this regard, the major source of error introduced by the homogenization theory can be attributed to the consideration of a limited number of unit cell repetitions, whereas the mathematical formulation of the homogenization theory assumes an infinite number of repetitions. This aspect is evident in Fig. 7, where relative differences between the analytical formulations and the FE analyses decrease as the number of unit cell repetitions increases in both the radial and axial directions. Additionally, other differences can be attributed to discretization errors introduced by the 3D FE model and by the numerical calculation of the material's homogenized tensor.

The analysis of the homogenized stiffness tensors in Eqs. (14), (17), (22) and (28) reveals important insights into the mechanical performance of the corresponding stents. For unit cell types 1 and 2, the components  $E_{1112}^H$  and  $E_{2212}^H$  are close to zero and markedly lower than  $E_{1111}^H$ ,  $E_{2222}^H$  and  $E_{1212}^H$ . This suggests that cells 1 and 2 exhibit approximately orthotropic material behavior, where normal and shear stress/strain coupling is negligible. Moreover, for unit cell type 2, the value of the component  $E_{1122}^H$  is close to zero, indicating a negligible coupling between normal stress/strain in circumferential and axial directions. Furthermore, since stiffness matrix components  $E_{1122}^H$  and  $E_{1111}^H$  have opposite sign, the foreshortening  $f$  is negative during radial compression, with the stent exhibiting an auxetic behavior (Eq. (14)). This feature is consistent with the study in [40] where a similar geometry is examined and classified as auxetic. Concerning unit cell type 3, component  $E_{1112}^H$  is negligible, whereas  $E_{2212}^H$  is of comparable magnitude with respect to  $E_{1111}^H$ ,  $E_{2222}^H$ , and  $E_{1212}^H$ . This suggests a potential coupling between normal and shear stress/strains, which may lead to

irregular closure of the stent during radial compression.

This study presents some limitations. The equations used to characterize the mechanical behavior of the stents are formulated under the assumption of linear elasticity. While this assumption has enabled the development of a rapid and automated method that can be easily integrated into different computational frameworks, it does not account for the large deformations experienced by the devices during crimping and subsequent expansion, and thus for geometric and material nonlinearity effects. It is important to note that the proposed method is well suited for the preliminary design phase of vascular stents and can be easily integrated into optimization frameworks, comparing the linear mechanical response of numerous stent designs and enabling the selective identification of set of ostensibly optimal stent unit cell geometries. Once these mechanically plausible stent designs are identified, a more in-depth analysis, combining computational and experimental tests, will be necessary to provide a comprehensive mechanical characterization of the new devices beyond the linear range. Furthermore, the method is developed by assuming the periodic repetition of the unit cell along the axial and circumferential direction of the stent, but vascular stents may feature a different periodic arrangement of links for axial connections of the unit cells, where not all unit cells are axially connected. While the specific periodic arrangement of the axial links may have a negligible impact on the stent radial stiffness [41], it could affect foreshortening, axial and torsional stiffness [42,43]. Lastly, only three loading scenarios were investigated, while other loading scenarios, such as bending, were not considered as the assumptions of plane stress and axial symmetry, used to define the analytical relationships, may not hold under these loading conditions. However, when other loading scenarios need to be addressed, the method can be adopted to design stents with unit cells optimized for radial stiffness, which are then connected by links specifically optimized for those additional loading conditions.

## 5. Conclusions

This study introduces a rapid and automated method based on homogenization theory for the derivation of analytical formulations for the assessment of the mechanical response of vascular stents starting from the associated unit cell topology. The method, successfully tested against FE simulations conducted on three stent designs with different unit cell types inspired to commercial vascular stents, proved to be accurate. The derived analytical formulations enable easy comparisons of the mechanical response of diverse stent designs under specific loading conditions (i.e., radial, axial traction and torsion loadings), and is well-suited for integration into several computational frameworks, including optimization frameworks. Overall, the presented approach has the potential to facilitate and refine the stent development process, reducing the time and costs associated with the iterative development and prototyping phases.

## CRedit authorship contribution statement

**Dario Carbonaro:** Conceptualization, Methodology, Software, Validation, Investigation, Formal analysis, Data curation, Visualization, Writing – original draft, Writing – review & editing. **Nicola Ferro:** Methodology, Investigation, Data curation, Writing – original draft, Writing – review & editing. **Francesco Mezzadri:** Methodology, Funding acquisition, Writing – original draft, Writing – review & editing. **Diego Gallo:** Methodology, Supervision, Writing – review & editing. **Alberto L. Audenino:** Resources, Supervision, Writing – review & editing. **Simona Perotto:** Methodology, Funding acquisition, Supervision, Writing – review & editing. **Umberto Morbiducci:** Conceptualization, Methodology, Supervision, Writing – review & editing. **Claudio Chiastra:** Conceptualization, Methodology, Supervision, Project administration, Funding acquisition, Writing – original draft, Writing –

review & editing.

## Declaration of competing interest

The authors declare that they have no known competing financial interests or personal relationships that could have appeared to influence the work reported in this paper.

## Funding

This study was carried out within the project “RESET: Rethinking femoral artery Stents for the trEatment of lower-limb peripheral arTery disease”, funded by the European Union – NextGenerationEU, Italian Ministry of University and Research, Italy, within the PRIN 2022 PNRR program (D.D.1409 del 14/09/2022). FM acknowledges the support of the research fund FAR 2023 DIP - Fondo di Ateneoper la Ricerca per il finanziamento di progetti di ricerca dipartimentali (Department of Engineering “Enzo Ferrari”, University of Modena and Reggio Emilia) and participates to the GNCS project MOMENTI - MOdelli e METodi Numerici per il Trattamento delle Immagini (Gruppo Nazionale per il Calcolo Scientifico - Istituto Nazionale di Alta Matematica “Francesco Severi”). NF and SP acknowledge the support by MUR, grant Dipartimento di Eccellenza 2023–2027. NF acknowledges the INdAM–GNCS 2024 Project “Accuratezza geometrica e adattività di griglia per problemi con interfacce complesse”.

## Acknowledgements

None.

## Supplementary materials

Supplementary material associated with this article can be found, in the online version, at [doi:10.1016/j.cmpb.2024.108467](https://doi.org/10.1016/j.cmpb.2024.108467).

## References

- [1] S. Borhani, S. Hassanajili, S.H. Ahmadi Tafti, S. Rabbani, Cardiovascular stents: overview, evolution, and next generation, *Prog. Biomater.* 7 (2018) 175–205, <https://doi.org/10.1007/s40204-018-0097-y>.
- [2] T.W. Duerig, M. Wholey, A comparison of balloon- and self-expanding stents, *Minim. Invasive Ther. Allied Technol.* 11 (2002) 173–178, <https://doi.org/10.1080/136457002760273386>.
- [3] W. Jiang, W. Zhao, T. Zhou, L. Wang, T. Qiu, A review on manufacturing and post-processing technology of vascular stents, *Micromachines* 13 (2022) 140, <https://doi.org/10.3390/mi13010140> (Basel).
- [4] C. Pan, Y. Han, J. Lu, Structural design of vascular stents: a review, *Micromachines* 12 (2021) 1–26, <https://doi.org/10.3390/mi12070770> (Basel).
- [5] B. Polanec, J. Kramberger, S. Glodež, A review of production technologies and materials for manufacturing of cardiovascular stents, *Adv. Prod. Eng. Manag.* 15 (2020) 390–402, <https://doi.org/10.14743/APEM2020.4.373>.
- [6] A. Kapoor, N. Jepson, N.W. Bressloff, P.H. Loh, T. Ray, S. Beier, The road to the ideal stent: a review of stent design optimisation methods, findings, and opportunities, *Mater. Des.* 237 (2024) 112556, <https://doi.org/10.1016/j.matdes.2023.112556>.
- [7] D. Carbonaro, E. Villa, D. Gallo, U. Morbiducci, A.L. Audenino, C. Chiastra, Designing the mechanical behavior of NiTi self-expandable vascular stents by tuning the heat treatment parameters, *J. Mech. Behav. Biomed. Mater.* 158 (2024) 106653, <https://doi.org/10.1016/j.jmbbm.2024.106653>.
- [8] A. García, E. Peña, M.A. Martínez, Influence of geometrical parameters on radial force during self-expanding stent deployment, Application for a variable radial stiffness stent, *J. Mech. Behav. Biomed. Mater.* 10 (2012) 166–175, <https://doi.org/10.1016/j.jmbbm.2012.02.006>.
- [9] F.D. Witcher, Simulation of in vivo loading conditions of nitinol vascular stent structures, *Comput. Struct.* 64 (1997) 1005–1011, [https://doi.org/10.1016/S0045-7949\(97\)00014-X](https://doi.org/10.1016/S0045-7949(97)00014-X).
- [10] A. Fortier, V. Gullapalli, R.A. Mirshams, Review of biomechanical studies of arteries and their effect on stent performance, *IJC Heart Vessels* 4 (2014) 12–18, <https://doi.org/10.1016/j.ijchv.2014.04.007>.
- [11] K. Maleckis, P. Deegan, W. Poulson, C. Sievers, A. Desyatova, J. MacTaggart, A. Kamenskiy, Comparison of femoropopliteal artery stents under axial and radial compression, axial tension, bending, and torsion deformations, *J. Mech. Behav. Biomed. Mater.* 75 (2017) 160–168, <https://doi.org/10.1016/j.jmbbm.2017.07.017>.
- [12] T.M. Morrison, M.L. Dreher, S. Nagaraja, L.M. Angelone, W. Kainz, The role of computational modeling and simulation in the total product life cycle of peripheral vascular devices, *J. Med. Devices Trans. ASME* 11 (2017) 1–10, <https://doi.org/10.1115/1.4035866>.
- [13] G. Alaimo, F. Auricchio, M. Conti, M. Zingales, Multi-objective optimization of nitinol stent design, *Med. Eng. Phys.* 47 (2017) 13–24, <https://doi.org/10.1016/j.medengphy.2017.06.026>.
- [14] S. Canić, L. Grubišić, D. Lacmanović, M. Ljulj, J. Tambača, Optimal design of vascular stents using a network of 1D slender curved rods, *Comput. Methods Appl. Mech. Eng.* 394 (2022) 1–32, <https://doi.org/10.1016/j.cma.2022.114853>.
- [15] D. Carbonaro, F. Mezzadri, N. Ferro, G. De Nisco, A.L. Audenino, D. Gallo, C. Chiastra, U. Morbiducci, S. Perotto, Design of innovative self-expandable femoral stents using inverse homogenization topology optimization, *Comput. Methods Appl. Mech. Eng.* 416 (2023) 116288, <https://doi.org/10.1016/j.cma.2023.116288>.
- [16] R. Clune, D. Kelliher, J.C. Robinson, J.S. Campbell, NURBS modeling and structural shape optimization of cardiovascular stents, *Struct. Multidiscip. Optim.* 50 (2014) 159–168, <https://doi.org/10.1007/s00158-013-1038-y>.
- [17] K.A. James, H. Waisman, Layout design of a bi-stable cardiovascular stent using topology optimization, *Comput. Methods Appl. Mech. Eng.* 305 (2016) 869–890, <https://doi.org/10.1016/j.cma.2016.02.036>.
- [18] N.S. Ribeiro, J. Folgado, H.C. Rodrigues, Surrogate-based multi-objective design optimization of a coronary stent: altering geometry toward improved biomechanical performance, *Int. J. Numer. Method. Biomed. Eng.* 37 (2021) 1–24, <https://doi.org/10.1002/cnm.3453>.
- [19] H.X. Li, W.L. Shi, Z. Tan, M.J. Wang, D.Y. Zhao, J. Yan, Topology optimization for polymeric stent, *Struct. Multidiscip. Optim.* 65 (2022) 1–13, <https://doi.org/10.1007/s00158-022-03292-z>.
- [20] S. Pant, G. Limbert, N.P. Curzen, N.W. Bressloff, Multiobjective design optimisation of coronary stents, *Biomaterials* 32 (2011) 7755–7773, <https://doi.org/10.1016/j.biomaterials.2011.07.059>.
- [21] S. Pant, N.W. Bressloff, G. Limbert, Geometry parameterization and multidisciplinary constrained optimization of coronary stents, *Biomech. Model. Mechanobiol.* 11 (2012) 61–82, <https://doi.org/10.1007/s10237-011-0293-3>.
- [22] W. Wu, D.Z. Yang, Y.Y. Huang, M. Qi, W.Q. Wang, Topology optimization of a novel stent platform with drug reservoirs, *Med. Eng. Phys.* 30 (2008) 1177–1185, <https://doi.org/10.1016/j.medengphy.2008.02.010>.
- [23] W. Wu, L. Petrini, D. Gastaldi, T. Villa, M. Vedani, E. Lesma, B. Previtali, F. Migliavacca, Finite element shape optimization for biodegradable magnesium alloy stents, *Ann. Biomed. Eng.* 38 (2010) 2829–2840, <https://doi.org/10.1007/s10439-010-0057-8>.
- [24] H. Xue, S.C. Saha, S. Beier, N. Jepson, Z. Luo, Topological optimization of auxetic coronary stents considering hemodynamics, *Front. Bioeng. Biotechnol.* 9 (2021) 1–17, <https://doi.org/10.3389/fbioe.2021.728914>.
- [25] H. Xue, Z. Luo, T. Brown, S. Beier, Design of self-expanding auxetic stents using topology optimization, *Front. Bioeng. Biotechnol.* 8 (2020) 1–16, <https://doi.org/10.3389/fbioe.2020.00736>.
- [26] D. Carbonaro, A. Lucchetti, A.L. Audenino, T. Gries, T.J. Vaughan, C. Chiastra, Multi-objective design optimization of bioresorbable braided stents, *Comput. Methods Programs Biomed.* 242 (2023) 107781, <https://doi.org/10.1016/j.cmpb.2023.107781>.
- [27] J.B. Russ, R.L. Li, A.R. Herschman, H. Waisman, V. Vedula, J.W. Kysar, D. Kalfa, Design optimization of a cardiovascular stent with application to a balloon expandable prosthetic heart valve, *Mater. Des.* 209 (2021) 109977, <https://doi.org/10.1016/j.matdes.2021.109977>.
- [28] D. Carbonaro, D. Gallo, U. Morbiducci, A. Audenino, C. Chiastra, In silico biomechanical design of the metal frame of transcatheter aortic valves: multi-objective shape and cross-sectional size optimization, *Struct. Multidiscip. Optim.* 64 (2021) 1825–1842, <https://doi.org/10.1007/s00158-021-02944-w>.
- [29] D. Carbonaro, S. Zambon, A. Corti, D. Gallo, U. Morbiducci, L. Audenino, C. Chiastra, Impact of nickel – titanium super-elastic material properties on the mechanical performance of self-expandable transcatheter aortic valves, *J. Mech. Behav. Biomed. Mater.* 138 (2023) 105623, <https://doi.org/10.1016/j.jmbbm.2022.105623>.
- [30] A. Bensoussan, J.L. Lions, G. Papanicolaou, Asymptotic Analysis for Periodic Structures, 2011. [doi:10.1090/chel/374](https://doi.org/10.1090/chel/374).
- [31] E. Andreassen, C.S. Andreasen, How to determine composite material properties using numerical homogenization, *Comput. Mater. Sci.* 83 (2014) 488–495, <https://doi.org/10.1016/j.commatsci.2013.09.006>.
- [32] N. Ferro, S. Perotto, D. Bianchi, R. Ferrante, M. Mannisi, Design of cellular materials for multiscale topology optimization: application to patient-specific orthopedic devices, *Struct. Multidiscip. Optim.* 65 (2022) 79, <https://doi.org/10.1007/s00158-021-03163-z>.
- [33] M. Gavazzoni, N. Ferro, S. Perotto, S. Foletti, Multi-physics inverse homogenization for the design of innovative cellular materials: application to thermo-elastic problems, *Math. Comput. Appl.* 27 (2022) 15, <https://doi.org/10.3390/mca27010015>.
- [34] N. Ferro, S. Micheletti, S. Perotto, Density-based inverse homogenization with anisotropically adapted elements. *Lectures Notes-Computer Science & Engineering*, Springer, 2020, pp. 211–221, [https://doi.org/10.1007/978-3-030-30705-9\\_19](https://doi.org/10.1007/978-3-030-30705-9_19).

- [35] ISO, Cardiovascular implants — Endovascular devices — Part 2: vascular stents, (2012).
- [36] FDA, Non-clinical Engineering Tests and Recommended Labeling For Intravascular Stents and Associated Delivery Systems, (2010).
- [37] G. Qi, C.X. Liu, K. Feng, L. Ma, K.U. Schröder, Analytical solutions of stress distribution within a hollow cylinder under contact interactions, *Int. J. Mech. Sci.* 239 (2023) 107897, <https://doi.org/10.1016/j.ijmecsci.2022.107897>.
- [38] F.P. Beer, R. Johnston, J. Dewolf, D. Mazurek, *Mechanics of Materials*, McGraw-Hill, 2013.
- [39] M.S. Cabrera, C.W.J. Oomens, F.P.T. Baaijens, Understanding the requirements of self-expandable stents for heart valve replacement: radial force, hoop force and equilibrium, *J. Mech. Behav. Biomed. Mater.* 68 (2017) 252–264, <https://doi.org/10.1016/j.jmbbm.2017.02.006>.
- [40] R. Vellaparambil, W. Han, P. Di Giovanni, S. Avril, Experimental validation of auxetic stent designs: three-point bending of 3D printed Titanium prototypes, 6 (2024) 1388207. [doi:10.3389/fmedt.2024.1388207](https://doi.org/10.3389/fmedt.2024.1388207).
- [41] M. Azaouzi, A. Makradi, S. Belouettar, F. Auricchio, R.L. Taylor, J. Lubliner, Numerical investigations of the structural behavior of a balloon expandable stent design using finite element method, *Comput. Methods Appl. Mech. Eng.* 72 (1997) 281–312, <https://doi.org/10.1016/j.commat.2013.01.031>.
- [42] X. Shen, K. Lu, H. Zhu, J. Jiang, R. Tian, H. Li, Torsional behavior of stents: the role of linker and stent tapering investigated with numerical simulation, *J. Mech. Med. Biol.* 22 (2022) 2250038, <https://doi.org/10.1142/S0219519422500385>.
- [43] A. Qiao, Z. Zhang, Solid and fluid simulations of vertebral artery stenosis treated with stents with different shapes of link, *Appl. Mech. Mater.* 553 (2014) 041007, <https://doi.org/10.4028/www.scientific.net/AMM.553.338>.